Journal of the Earth and Space Physics, Vol. 44, No. 4, Winter 2019, P. 99-114
DOI: 10.22059/jesphys.2018.245567.1006940

Application of Wavelet Neural Networks for Improving of Ionospheric Tomography Reconstruction over Iran

Ghaffari Razin, M. R.[1*] and Voosoghi, B.[2]

1. Assistant Professor, Department of Surveying Engineering, Arak University of Technology, Arak, Iran
2. Associate Professor, Department of Geodesy, Faculty of Geodesy and Geomatics Engineering, K. N. Toosi Univ. of Technology, Tehran, Iran

(Received: 20 Nov 2017, Accepted: 25 Sep 2018)

Abstract
In this paper, a new method of ionospheric tomography is developed and evaluated based on the neural networks (NN). This new method is named ITNN. In this method, wavelet neural network (WNN) with particle swarm optimization (PSO) training algorithm is used to solve some of the ionospheric tomography problems. The results of ITNN method are compared with the residual minimization training neural network (RMTNN) and modified RMTNN (MRMTNN). In all three methods, empirical orthogonal functions (EOFs) are used as a vertical objective function. To apply the methods for constructing a 3D-image of the electron density, GPS measurements of the Iranian permanent GPS network (in three days in 2007) are used. Besides, two GPS stations from international GNSS service (IGS) are used as test stations. The ionosonde data in Tehran (φ=35.73820, λ=51.38510) has been used for validating the reliability of the proposed methods. The minimum RMSE for RMTNN, MRMTNN, ITNN are 0.5312, 0.4743, 0.3465 (10^{11}ele./m^3) and the minimum bias are 0.4682, 0.3890, and 0.3368 (10^{11}ele./m^3) respectively. The results indicate the superiority of ITNN method over the other two methods.

Keywords: Tomography, RMTNN, MRMTNN, ITNN, GPS.

1. Introduction
In the last two decades, knowledge of the distribution of the ionospheric electron density is considered as a major challenge for geodesy and geophysics researchers. To study the physical properties of the ionosphere, tomography indicated an efficient and effective method. Usually the value of total electron content (TEC) used as an input parameter to tomography. Then, inversion methods used to compute the electron density at any time and space. However, ionospheric tomography is considered as an inverse ill-posed problem due to the lack of input observations and non-uniform distribution of TEC data.

Tomography is a mathematical technique to reconstruct three-dimensional images and is best known for the reconstruction of the human body from the X-ray measurements (Amerian et al., 2010). Many algorithms and methods are presented for modeling the ionospheric tomography. For the first time, Austen et al. (1988) proposed the idea of using satellite radio tomography to study the ionospheric electron density. After that, reconstruction of the ionospheric electron popular and successful way of studying the detailed features of the ionosphere. Extensive research in ionospheric tomography offers several advantages over traditional ground-based instruments such as incoherent backscatter radars and ionosonde. Kunitsyn et al. (2011) used ionospheric radio tomography based on data from high orbital navigation systems. The minimum Sobolev's norm was suggested for finding the solution. Pokhotelov et al. (2011) used 4D tomography reconstruction to detect the ionosphere anomalies in the high-latitude polar cap region. Wen et al. (2012) presented a new tomographic algorithm, termed two-step algorithm (TSA). In this method, electron density is estimated in two steps: Phillips smoothing method (PSM) is used to resolve the ill-conditioned problem and the PSM solution is input as an initial value to the algebraic reconstruction technique. Van de Kamp (2013) examined the ionosphere above Scandinavia by 4-dimensional tomography using the software package MIDAS from the University of Bath. Ghaffari Razin (2015) expanded 3D ionosphere tomography by

*Corresponding author: mr.ghafari@arakut.ac.ir

empirical orthogonal functions. The zero order Tikhonov regularization used for parameter estimations. Ghaffari Razin and Voosoghi (2016) developed local ionosphere tomography model over Iran using spherical cap harmonics (SCHs).

Although the results of all studies indicate high efficiency of ionospheric tomography, two major limitations can be considered to this method: First, due to the poor spatial distribution of GPS stations and limitations of signal viewing angle, computerized ionospheric tomography (CIT) is an inverse ill-posed problem. Second, in most cases, observations are discontinuous in time and space domain; therefore, it is not possible determining the density profiles at any time and space around the world. For solving the mentioned problems, it is necessary to extend a suitable local model with high spatial-temporal resolution that uses GNSS observations. Artificial neural networks (ANNs) are one of the new ideas to solve the mentioned problems.

ANN is a set of information processing system that has been formed by simple processing elements called artificial neurons. Methods of artificial intelligence provide a valuable tool for modeling of the nonlinear behavior of the ionosphere (Habarulema et al., 2009; Yilmaz et al., 2009; Ghaffari Razin et al., 2015). For the first time, Ma et al. (2005) demonstrated the idea of using an ANNs to solve the ionospheric tomography. They used standard ANN (SANN) with back-propagation (BP) algorithm to train the network. Besides, they used ionosonde observations for improving the vertical resolution. After it, Hirooka et al. (2011) used the same ANN for modeling the ionospheric electron density distributions. They used low earth orbit (LEO) observations as vertical constraints and updated neural weights using these information. Low accuracy in the vertical domain is the major disadvantage of these two studies. In order to solve the low accuracy in vertical domain, Ghaffari Razin and Voosoghi (2016) used empirical orthogonal functions (EOFs) as vertical constraints. Despite the improvement in the vertical accuracy due to the use of EOF, accuracy of time domain is low.

The goal of this paper is to develop and evaluate a new method of ionosphere tomography using wavelet neural network (WNN) and particle swarm optimization (PSO) training algorithm. This new method called ionospheric tomography based on the neural networks (ITNN). Using this method, it is possible to obtain the ionospheric electron density temporal and spatial variations in high accuracy and resolution. Besides, total electron content (TEC) in any desired positions can be computed. All of the results in this paper compared with the residual minimization training neural network (RMTNN) and modified RMTNN (MRMTNN). SANN and WNN have been used as base neural networks (NNs). Back-propagation (BP) and particle swarm optimization (PSO) algorithms are used for training these methods. Observations of three days in 2007 (2007.01.03, 2007.04.03 and 2007.07.13) is selected to apply the methods. To validate and better assess the reliability of the proposed method, two GPS stations from international GNSS service (IGS) are used as test stations. The accuracy of the results is controlled with Tehran ionosonde measurements. Statistical indicators as, root mean square error (RMSE), bias and dVTEC (reconstructed $_{\mathrm{TEC}}$ − observed $_{\mathrm{TEC}}$) are used to assess the results.

2. **Measurements**

Using ground–based GPS receivers, it is possible to compute slant TEC (STEC), that is one of the most important data sources in ionospheric researches. Carrier phase derived STEC ($\mathrm{STEC_L}$) and code pseudo- ranges STEC ($\mathrm{STEC_P}$) are calculated with the following equations:

$$STEC_L = \frac{(f_1 f_2)^2}{40.3\left(f_1^2 - f_2^2\right)}\left(L_1\lambda_1 - L_2\lambda_2\right) \quad (1)$$

$$STEC_P = \frac{(f_1 f_2)^2}{40.3\left(f_1^2 - f_2^2\right)}\left(P_2 - P_1\right) \quad (2)$$

where f_1 and f_2 are signal frequency, L_1 and L_2 are the carrier phase measurements, λ_1 and λ_2 are the wavelengths, P_1 and P_2 are the code pseudo- ranges measurements. Carrier phase derived $STEC_L$ depending on the ambiguity parameters while the code derived $STEC_P$ observation is noisy.

To reduce the multipath and noise level in the $STEC_P$, the carrier phase measurements are used to compute a more precise relative STEC observable. In this approach, the continuous arcs of $STEC_L$ are adjusted to the mean value of the corresponding code $STEC_P$ value. The mean value is computed for every continuous arc using:

$$\left\langle STEC_P + STEC_L \right\rangle = \frac{1}{N}\sum_{i=1}^{N}\left(STEC_P + STEC_L\right)_i \quad (3)$$

where N is the number of continuous measurements contained in the arc. Subtracting Equation (1) from (3), the smoothed STEC can be derived:

$$\begin{aligned} &STEC_{smoothed} = \\ &\left\langle STEC_P + STEC_L \right\rangle - STEC_L = \\ &STEC + \left(B_r^P + B_s^P\right) + \varepsilon_{P4} \end{aligned} \quad (4)$$

where B_r^P and B_s^P are the receiver and satellite code-delay inter-frequency bias (IFB) in TECU (10^{16} ele./m^2) respectively, and ε_{P4} is the combination of multipath and measurement noise on P_1 and P_2 in TECU (10^{16} ele./m^2).

3. Ionospheric tomography using neural networks

ANNs have demonstrated to be an ideal tool for the prediction of ionospheric variations (time and space dependent), which is by nature highly non-linear. A main benefit of using ANNs for the prediction of ionospheric variations
over analytical methods is that no previous information of the nature of the non-linear relationships is needed. The first idea of using ANNs in the ionospheric tomography was provided by Ma et al., (2005). They used the method described by Liaqat et al., (2003) namely residual minimization training neural network (RMTNN). In the next section, this method will be explained briefly.

3-1. Residual minimization training neural network (RMTNN)

STEC as the integrated value of the ionospheric and plasmaspheric electron density can be calculated using Equation (5):

$$STEC_{smoothed} = \int_r^s N(\vec{r},t)ds + P_r^s \quad (5)$$

where $N(\vec{r},t)$ shows the electron density at the position $\vec{r}$ and observational time t, P_r^s is the contribution of the plasmaspheric electron density, r and s indicate total number of receivers and satellites, respectively. Computational domain is divided ionospheric region (100 km to 1000 km) and plasmaspheric region (above 1000 km). With discretize of Equation (5) can be written:

$$STEC_{smoothed} \approx \sum_{d=1}^{D}\beta_d N(\vec{r},t) + P_r^s \quad (6)$$

where d show a mesh point (the symbol D is the total number of the mesh points) and β corresponding weight in the numerical integration. To see the role of β in numerical integration, please refer to Quarteroni et al. (2007, Chapter 9). Using Equation (6), it can be defined the cost function as follows:

$$C_1 = \left(\sum_{d=1}^{D}\beta_d N(\vec{r},t) + P_r^s - STEC_{smoothed}\right)^2 \quad (7)$$

The most significant drawback of the ionospheric tomography is low accuracy in the vertical domain. To compute the vertical cost function, empirical orthogonal functions (EOFs) is used. Using this method, the neural network is trained and the vertical cost function is given as:

$$C_2 = \sum_{g=1}^{G}\left(N_g(\vec{r}) - N_g^{EOF}\right)^2 \quad (8)$$

where G is the number of EOF, $N_g(\vec{r})$ is the output of the neural network, and N_g^{EOF} is the EOF$_S$ electron density for the position (r). Thus, the total cost function is considered as follows:

$$C = bC_1 + C_2 \quad (9)$$

where b is a balance parameter between the EOFs and GPS results. To select the value of b, the amount of error in the cost function C is used. If the value of cost function C is below 2×10^{11} (ele./m^3), the neural network is converged to the optimal result. This value has been empirically determined. As a result,

b = 0.94 is selected as the balance parameter. The weight updating process of the neural network for the cost functions C_1 and C_2 is derived for the nth path as follows:

$$\Delta w = -\eta \frac{\partial C_1}{\partial w} \approx -\eta \sum_{d=1}^{D} \left(I_n^{NN} + P_r^s - I_n\right) \frac{\partial I_n^{NN}}{\partial N^d} \frac{\partial N^d}{\partial w} \approx -\eta \sum_{d=1}^{D} \left(I_n^{NN} + P_r^s - I_n\right) \beta_d \frac{\partial N^d}{\partial w} \quad (10)$$

$$\Delta w = -\eta \frac{\partial C_2}{\partial w} \approx -\eta \sum_{g=1}^{G} \left(N_g(\vec{r}) - N_g^{EOF}\right) \quad (11)$$

Where n indicates the ray path, I_n^{NN} is the output data of the neural network, I_n is the real data (obtained using Equation 6), the weight of the main neural network is w and η is the learning rate.

3-2. Modified residual minimization training neural network (MRMTNN)

In the RMTNN method, SANN is used. The standard sigmoid ANNs have a series of disadvantages. Typically, the initial weights of the ANN are randomly selected in these networks. Randomly chosen initial weights of network are increasing significantly training time. Moreover, when the activation function is of sigmoidal type, there is always remarkable change that the training algorithm will converge to local minima. Finally, there is no logical connection between the activation function, optimal network structure and the complexity of the mathematical model. Therefore, instead of using the conventional sigmoid activation functions can be used wavelet neural network. The WNN employing non-linear wavelet basis functions (named wavelets), which are localized in both the time and frequency space, has been extended as an alternative approach to non-linear fitting problem (Alexandridis and Zapranis, 2013). In WNNs the network output is given by Equation (12):

$$g_\lambda(\mathbf{x};\mathbf{w}) = \hat{y}(\mathbf{x}) = \omega_{\lambda+1} + \sum_{j=1}^{\lambda} \omega_j . \Psi_j(\mathbf{x}) + \sum_{i=1}^{m} \omega_i . x_i \quad (12)$$

where $\mathbf{x}$ is the input vector, $\Psi_j(\mathbf{x})$ is a multi-dimensional wavelet that is constructed by the product of m scalar wavelets, $\boldsymbol{m}$ is the number of inputs, $\boldsymbol{\lambda}$ is the number of hidden units and ω shows for a network weight. Multi-dimensional wavelets can be calculated by Equation (13):

$$\Psi_j(\mathbf{x}) = \prod_{i=1}^{m} \psi(z_{ij}) \quad (13)$$

Where ψ is the mother wavelet and can be written as:

$$z_{ij} = \frac{x_i - a_{ij}}{b_{ij}} \quad (14)$$

In Equation (14), $i = 1,...,m$, $j = 1,...,\lambda + 1$ and the weights ω is related to the translation (a_{ij}) and the dilation (b_{ij}) parameters. The choice of the mother wavelet depends on the applications. The activation function can be considered orthogonal wavelets (wavenet) or continuous wavelets (wave frame). In this paper, the Mexican hat function is used as a mother wavelet. This wavelet has many benefits and shown satisfactory results in other applications. Analytical form of the Mexican hat function is as follows:

$$\psi(z_{ij}) = \left(1 - z_{ij}^2\right) e^{-\frac{1}{2} z_{ij}^2} \quad (15)$$

For optimizing the initialization of the wavelet parameters, various methods have been proposed. The translation and dilation parameters are used as follows (Zhang and Benveniste, 1992):

$$a_{ij} = 0.5\left(N_i + M_i\right) \quad (16)$$

$$b_{ij} = 0.2\left(M_i - N_i\right) \quad (17)$$

where N_i and M_i are defined as the minimum and maximum of input $\mathbf{x}_i$.

3-3. Ionospheric tomography based on the neural network (ITNN)

The usually used training algorithm for ANN and WNN is back-propagation (BP) algorithm, which is a gradient-based method. The BP algorithm easily falls into the trap of

local minima, especially for complex function approximation problem. Therefore, the BP algorithm is weak to find a global optimal solution. Besides, the speed of convergence to the optimal solution is very low in this algorithm. Other key issues in this algorithm can be considered: dependence on the initial values of the weights, as well as the optimal selection of the parameters such as the learning rate and the momentum. This disadvantage can be removed by an exploration ability of the evolutionary algorithms such as particle swarm optimization (PSO). For the first time, Kennedy and Eberhart (1995) proposed the PSO algorithm as a population-based optimization method. A PSO algorithm is inspired by the movements of the best member of the population and at the same time by their own experience. This metaphor indicates that a set of solutions is moving in a search space with the aim to achieve the best position or solution. Table 1 demonstrates the PSO learning algorithm.

In Table 1, **P** is the particle swarm, $\mathbf{x}_i$ is the position of a particle, $\mathbf{v}_i$ is the velocity of a particle, $\otimes$ is component-wise multiplication, and $\mathbf{U}(0,\phi_i)$ is a random numbers vector uniformly distributed in the interval $[0,\phi_i]$. Unlike BP, PSO is a global search and population-based algorithm used for training neural networks, finding neural network architectures, tuning network learning parameters and optimizing network weights. PSO avoids trapping in a local minimum, because it is not based on gradient information. The equations used in this algorithm are considered as follows:

$$v_i^{t+1} = w \times v_i^t + c_1 \times rand \times \left(pbest_i - x_i^t\right) + c_2 \times rand \times \left(gbest - x_i^t\right) \quad (18)$$

$$x_i^{t+1} = x_i^t + v_i^{t+1} \quad (19)$$

Where w is inertia weight, v_i^t is the velocity of particle i at iteration t, c_1 and c_2 are acceleration coefficients, *rand* is a random number within [0,1], x_i^t defines the current location of particle i at iteration t, $pbest_i$ demonstrates the *pbest* of factor i at iteration t, and *gbest* is the best solution so far. In each iteration, the velocities of particles are calculated by Equation (18). Then, the locations of particles are computed by Equation (19). The particle positions will be varied until a stopping condition is met.

Table 1. The PSO algorithm.

Particle Swarm Optimization (PSO) Algorithm
  Create and initialize particles
  repeat
    For all $x_i \in P$ do
      Compute fitness of particle $f(x_i)$
      If $f(x_i) < f(p_i)$ then
        $p_i = x_i$
      End if
      If $f(x_i) < f(p_g)$ then
        $p_g = x_i$
      End if
      $v_i = \omega v_i + U(0,\phi_1) \otimes (p_i - x_i) + U(0,\phi_2) \otimes (p_g - x_i)$
      $x_i = x_i + v_i$
    End for
Until termination criterion is met

4. Error evaluation:

In this paper, results were analyzed based on root mean square error (RMSE) and bias. These two indices are calculated as follows:

$$RMSE = \sqrt{\frac{1}{N}\sum_{i=1}^{N}\left(N_R - N_{ionosonde}\right)^2} \qquad (20)$$

$$Bias = \frac{1}{N}\sum_{i=1}^{N}\left(N_R - N_{ionosonde}\right) \qquad (21)$$

Where N_R is the reconstructed value of electron density using RMTNN, MRMTNN and ITNN, $N_{ionosonde}$ is the observed value of electron density from ionosonde, and N is the number of sample elements. Moreover, after reconstructed electron density using RMTNN, MRMTNN and ITNN methods, vertical total electron content (VTEC) is computed and compared with the corresponding VTEC that is obtained from GPS measurements:

$$dVTEC = VTEC_{GPS} - VTEC_M \qquad (22)$$

where $VTEC_{GPS}$ shows VTEC computed by GPS measurements and $VTEC_M$ indicates VTEC that is reconstructed by RMTNN, MRMTNN and ITNN methods.

5- Results and discussions:

Geodynamic studies in Iran began since 1998. The main objective of these studies was to investigate variations in the Earth's crust and tectonic movement. Iran permanent GPS network was designed and implemented gradually from 2004. Using the permanent GPS network, it was created to study the mechanism of the active faults. Iranian permanent GPS network (IPGN) contains 120 settled GPS stations spread all over Iran, and it provides a perfect tool for analyzing ionospheric properties over Iran. IPGN data contains pseudo range (P_1, P_2) and phase (L_1, L_2) data for two different frequency bands transmitted from GPS satellites (L_1 and L_2 bands). From these 120 stations, 36 stations are selected for three days of 2007 (2007.01.03, 2007.04.03 and 2007.07.13) for modeling ionospheric electron density. In order to better assess the validity of the proposed model, two testing stations (TEHN (35.41^0_N, 51.20^0_E), BHR4 (26.12^0_N, 50.36^0_E)) from IGS tracking stations have been selected. Testing stations have been chosen so that proper assessment can be made. The distributions of these receivers are given in Figure 1. These stations are marked with circles in Figure 1. As shown in Figure 1, one ionosonde station (Tehran (35.87^0_N, 51.64_E)) is located in the research area. Thus, there is the possibility of a more accurate evaluation for three models.

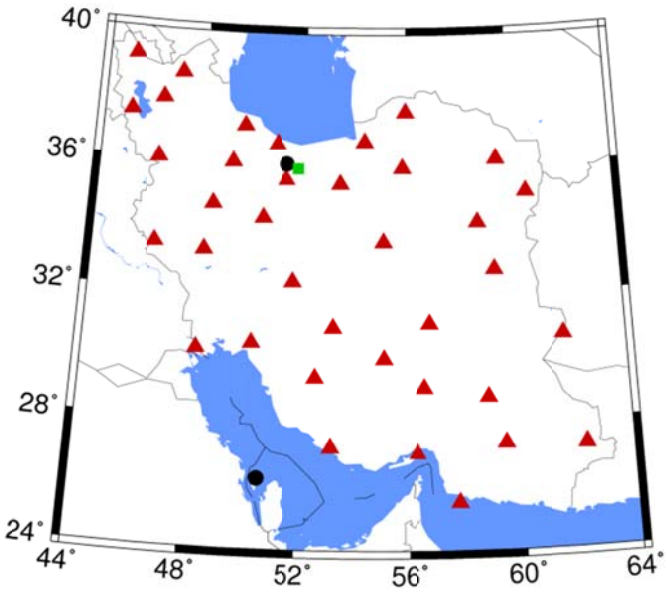

Figure 1. The distribution of GPS, IGS and ionosonde stations in Iran (triangles show GPS stations, circles indicate IGS tracking stations and green square is the ionosonde station).

To perform calculations, spatial resolution is selected 0.50×0.50×50 (Km) along the longitude, latitude and altitude. Thus, the total numbers of voxels are 23040. Besides, half-hour GPS observation data is used to do processing in all experiments. On the other words, observation time interval selected half-hour. Using data from space weather prediction center, these days are calm and geomagnetic indices are shown in Figure 2.

The performance of the proposed methods (RMTNN, MRMTNN and ITNN) is compared in terms of network structure, number of iteration and time of convergence to the optimal solution. Table 2 shows the comparison. All processing and computing is done on the same computer system (MATLAB 8.5.0 using a 2.4 GHz PC equipped with 8 GB of random access memory run by windows 8.1). It should be noted that after extensive testing, the 4-18-1 structure was selected as the optimum structure for all three methods. In training part of all three methods (RMTNN, MRMTNN and ITNN), input space included four observations used to train and obtain the variations of the ionospheric electron density. Therefore, the predicted N is a function of four inputs and can be simply expressed mathematically according to the following expression:

$$N_R = f\left(latitude \quad longitude \quad altitude \quad time\right) \tag{23}$$

Using the results presented in Table 2, the difference between the methods becomes apparent. The time of convergence to the optimal solution and number of iteration in ITNN method is less than the MRMTNN and RMTNN methods. Time of convergence to the optimal solution is considerably reduced in ITNN method with respect to RMTNN method (original method). This result reflects the fact that using WNN with PSO training algorithm (ITNN method) computation speed is increased. Table 3 shows the average RMSE and bias values for ionosonde station in four selected heights (200, 250, 300 and 350 Km) at three days (2007.01.03, 2007.04.03 and 2007.07.13). It should be noted that RMSE is often used to verify the reliability of the proposed method. Using this table, it is possible to compare the results obtained from each method.

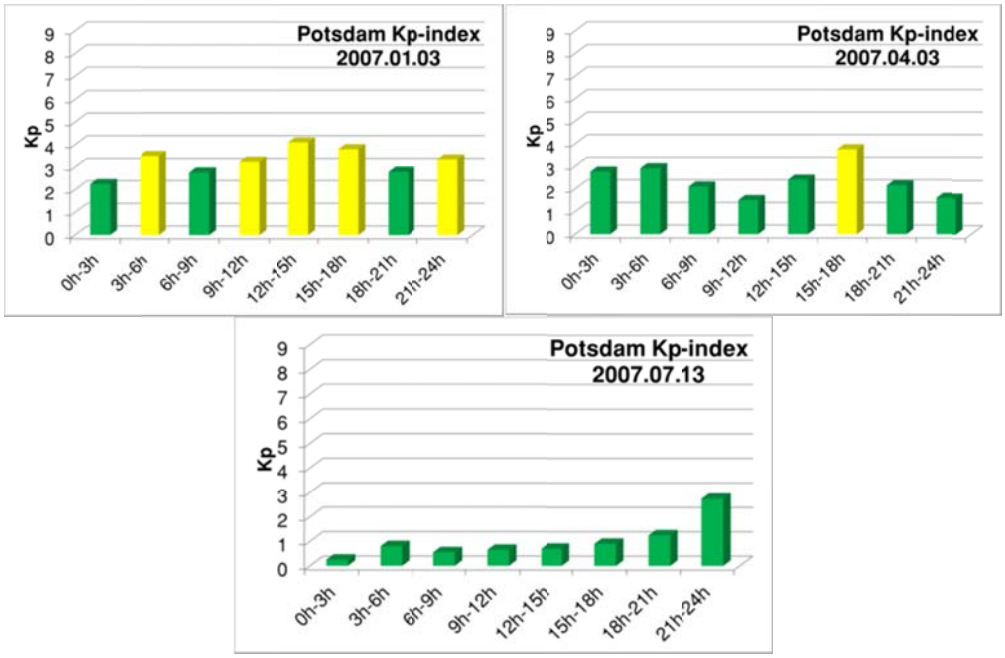

Figure 2. Kp index for three days of 2007 (http://www.spaceweatherlive.com/en/archive/2007).

Table 2. Comparison of the network structure, number of iteration and time for convergence in RMTNN, MRMTNN and ITNN methods.

Reconstruction methods	Network Structure (input, hidden, output)	No. of iterations	Time of convergence (second)
RMTNN	4-18-1	1321	645
MRMTNN	4-18-1	1215	610
ITNN	4-18-1	1053	579

Table 3. Average RMSE and bias comparison in four selected heights (200, 250, 300 and 350 Km) at 2007.01.03, 2007.04.03 and 2007.07.13 over ionosonde station.

Days	RMTNN		MRMTNN		ITNN	
	RMSE	Bias	RMSE	Bias	RMSE	Bias
	10^{11} ele./m^3		10^{11} ele./m^3		10^{11} ele./m^3	
2007.01.03	0.54	0.51	0.51	0.47	0.44	0.40
2007.04.03	1.29	1.009	0.86	0.63	0.67	0.50
2007.07.13	1.26	1.05	0.42	0.38	0.27	0.25

The results in Table 3 demonstrate that the RMSE and bias of ITNN method is less than the other two methods. It means that by using WNN with PSO training algorithm, accuracy of the method is considerably increased. On the other hand, in comparison with the original method (RMTNN), the ITNN method is improved electron density reconstruction. It should be noted that even MRMTNN method is also more accurate than the RMTNN method. In the other words, by varying the SANN to WNN, results improved.

In order to better evaluate RMTNN, MRMTNN and ITNN reconstruction methods, VTEC values in three days and two testing stations is computed. Then, these values (reconstructed VTEC) compared with the VTEC obtained from GPS measurements ($VTEC_{GPS}$) and IRI-2012 VTEC ($VTEC_{IRI\text{-}2012}$). Equation (22) is used for this purpose. This measure can provide a means for the direct comparison of the obtained results spatially and temporally. Figure 3 shows the results of these computations.

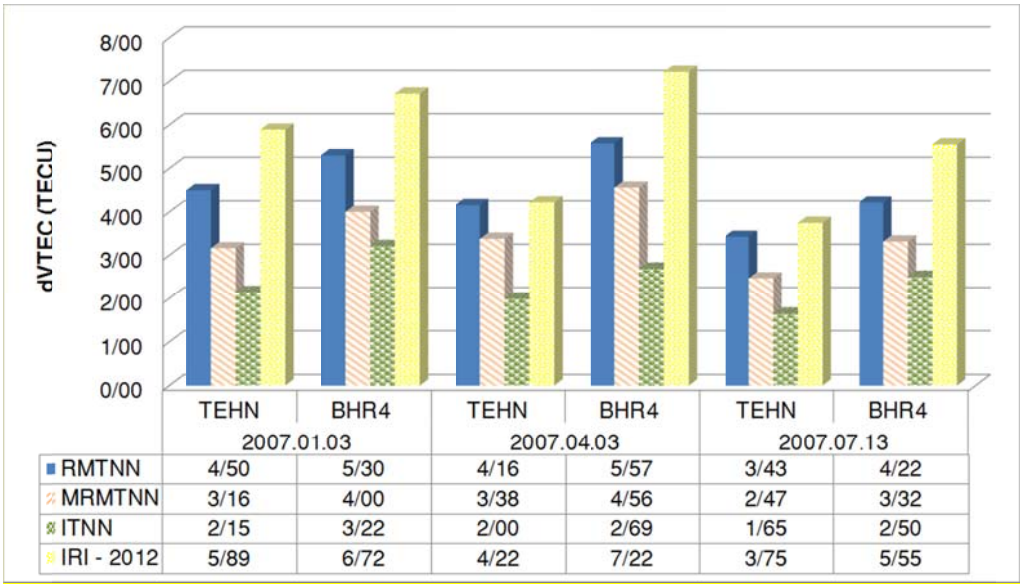

Figure 3. Comparison of daily average of dVTEC (TECU) in three days for RMTNN, MRMTNN, ITNN and IRI-2012 methods over two testing stations (TEHN and BHR4).

Using results in Figure 3, it can be seen clearly that the results of the ITNN ($VTEC_{ITNN}$) method are much closer to the results of the GPS observations ($VTEC_{GPS}$). In the other words, the numerical value of the dVTEC in ITNN method is much less than other methods. Another important point, it can be investigated in Figure 3, is low accuracy of the results of the IRI-2012 model. The IRI-2012 model used ionosonde observations for modeling the ionosphere variations. Due to the small number of these stations in the world, the results of this model are not accurate. For analyzing the accuracy of the methods in ionospheric electron density reconstruction, results compare with ionosonde direct measurements. Figure 4 indicates the scatter plot for RMTNN, MRMTNN and ITNN electron density with corresponding electron density from the ionosonde in three days of 2007 with lines of best fit showed for all cases.

Using Figure 4, it is clearly visible that the ITNN method is highly correlated to ionosonde measurements with a correlation coefficient (R) of 0.901. The values of correlation coefficient between MRMTNN and RMTNN with ionosonde measurements are 0.860 and 0.826, respectively. These results again indicate that the original ionospheric reconstruction method (RMTNN) is improved. After assessing the accuracy of the proposed methods, it is possible to draw profiles of time-dependent ionosphere electron density. The results of this analysis are shown in Figures 5, 6 and 7. In these figures, reconstructed electron density profiles using RMTNN, MRMTNN and ITNN were compared with ionosonde profiles. All these comparisons have been conducted for heights of 200, 250, 300 and 350 Km in three days of 2007 (2007.01.03, 2007.04.03 and 2007.07.13). Using these figures, it is obvious that the peak of electron density occurs in 08:00 to 10:00 UT, and also temporal variation of ionospheric electron density can be seen clearly.

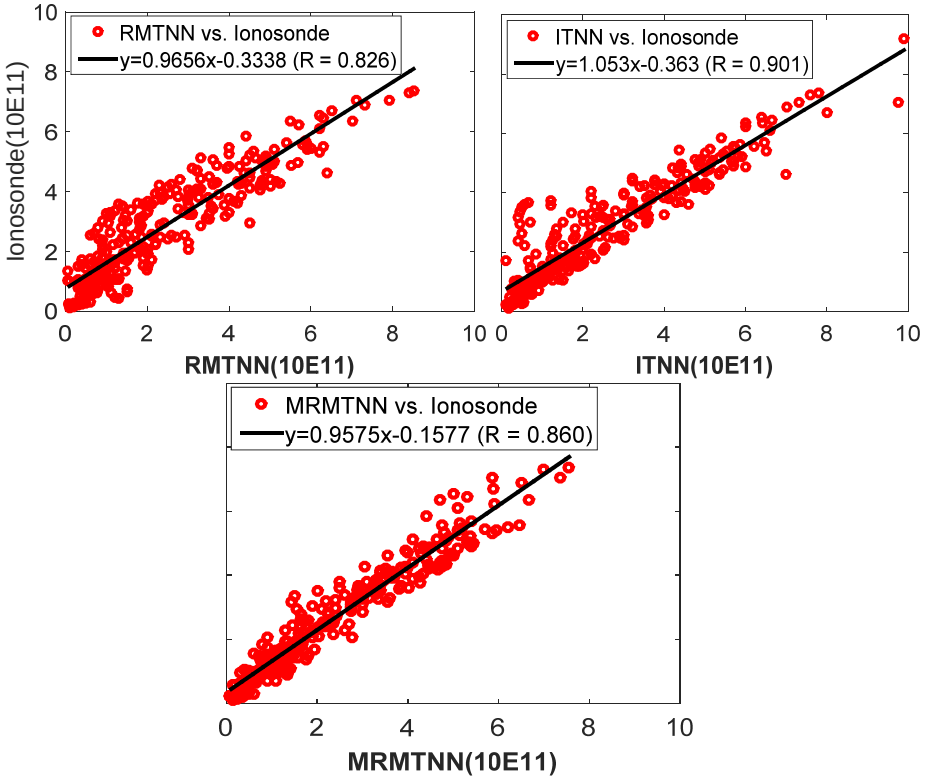

Figure 4. Scatter plots for ionosonde electron density and corresponding reconstructed electron density values using RMTNN (left panel), MRMTNN (middle panel) and ITNN (right panel) in three days of 2007.

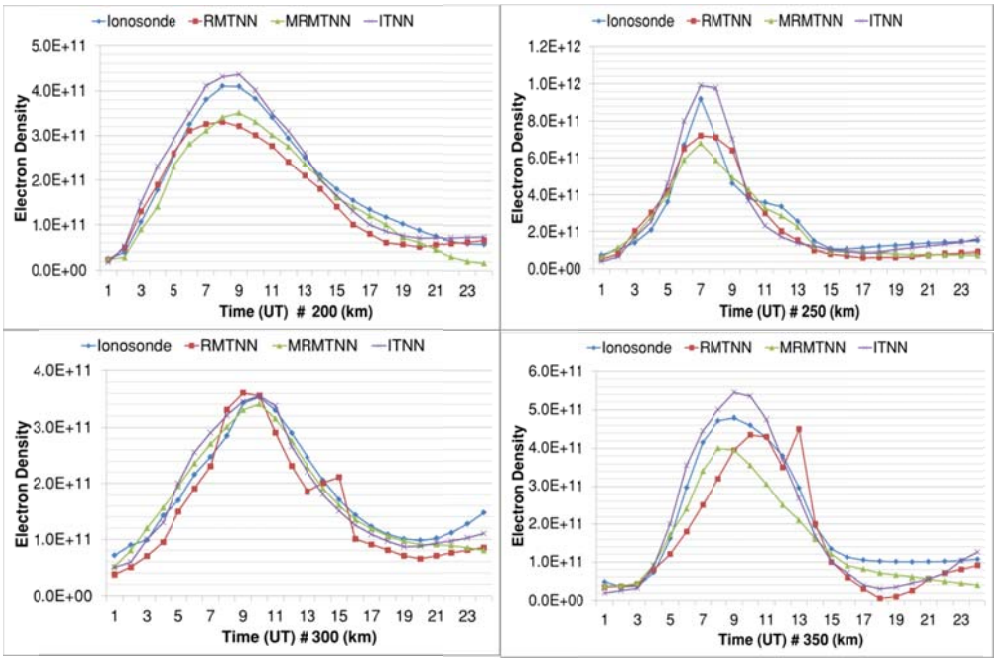

Figure 5. Comparison of ionosonde, RMTNN, MRMTNN and ITNN electron density variation in four selected altitudes (200, 250, 300 and 350 Km) over ionosonde station at 2007.01.03.

According to the results of Figure 5, ITNN electron density profiles are very close to the ionosonde electron density profiles. This fact can be seen in Figures 6 and 7. Figure 6 shows the comparison for the 2007.04.03.

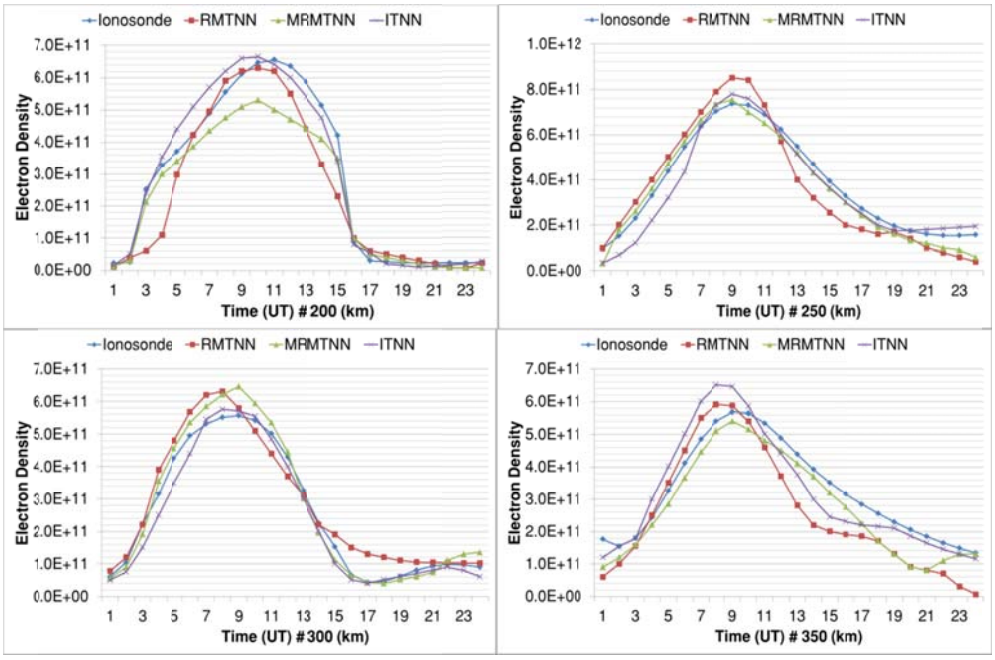

Figure 6. Comparison of ionosonde, RMTNN, MRMTNN and ITNN electron density variation in four selected altitudes (200, 250, 300 and 350 Km) over ionosonde station at 2007.04.03

Figure 7 shows temporal variations of ionospheric electron density in four selected altitude (200, 250, 300 and 350). Again (similar to Figures 4 and 5), the outputs of ITNN method are closer to the results of ionosonde compared with RMTNN and MRMTNN.

The 3-dimensional images of the RMTNN, MRMTNN and ITNN spatial distributions of vertical electron density are shown in Figure 8. These figures are drawn at a fixed longitude of 55^0 E for a vertical cross section. All figures are drawn at 12:00 UT. The top panel is for the 2007.01.03, middle panel is for the 2007.04.03 and bottom panel is for the 2007.07.13.

In Figure 8, the difference is obvious between three ionospheric reconstruction methods. Using Figure 8, vertical variations of ionospheric electron density can be seen clearly. Besides in all methods (RMTNN, MRMTNN and ITNN), the maximum electron density occurred at an altitude of 250:350 kilometers. Moreover, daily variation in the height of maximum electron density is remarkable in these results. This corresponds to the expected diurnal variations of electron density. These characteristics that are the constituents of the ionosphere morphology in three dimensions are also reported elsewhere (Yizengaw et al., 2007) and confirmed by the analysis of the direct measurement techniques.

Figures 9, 10 and 11 illustrate the horizontal variations of VTEC over the study area in three days of 2007.01.03, 2007.04.03 and 2007.07.13 suggested by the ITNN method (in 10^{16} ele./m^2). All figures drawn at four time interval: two times in day-side and two times in night-side. The main purpose of drawing these maps is indicating the horizontal variations in ionosphere electron content.

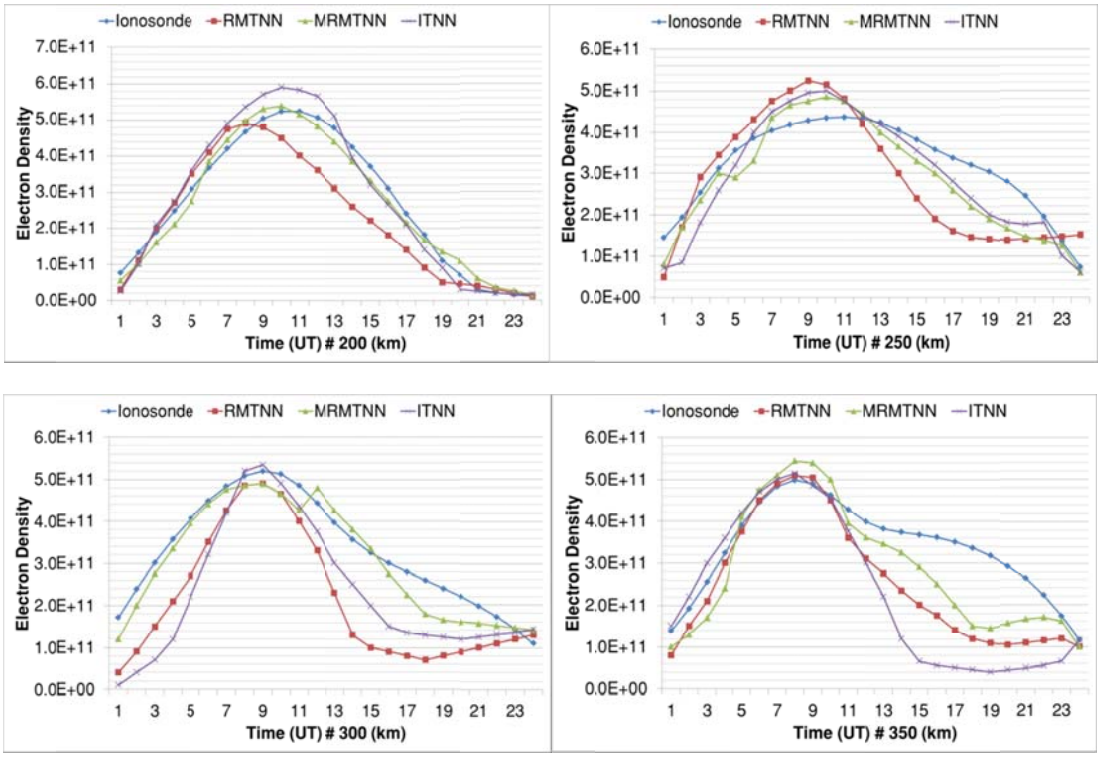

Figure 7. Comparison of ionosonde, RMTNN, MRMTNN and ITNN electron density variation in four selected altitudes (200, 250, 300 and 350 Km) over ionosonde station at 2007.07.13.

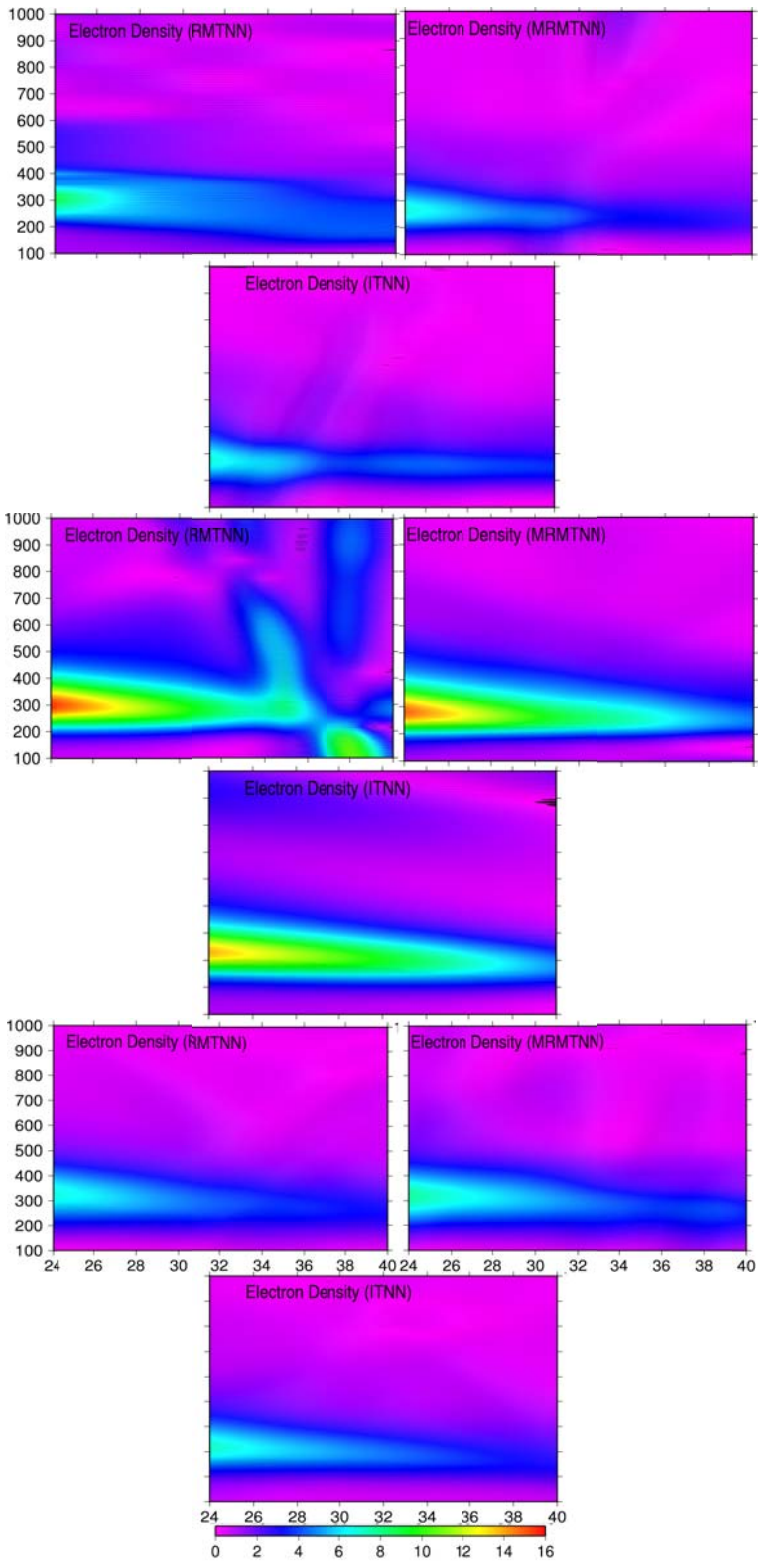

Figure 8. Ionospheric electron density distribution at longitude 55° E in10^{11} ele./m^3 using RMTNN, MRMTNN and ITNN methods in 2007.01.03 (top panel), 2007.04.03 (middle panel) and 207.07.13 (bottom panel).

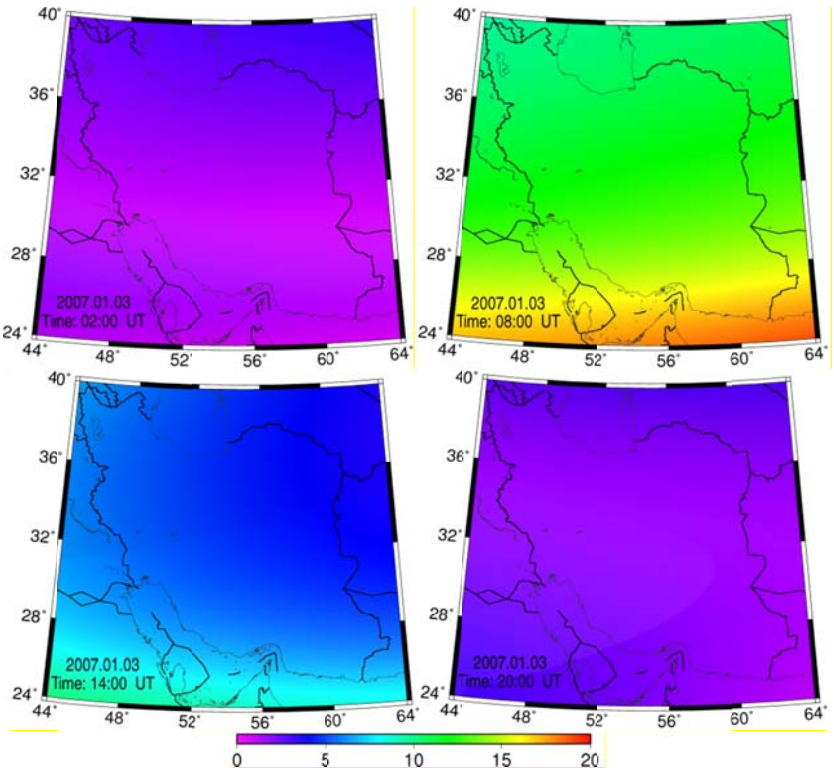

Figure 9. The model estimates of VTEC (10^{16} ele./m^2) at four times in 2007.01.03.

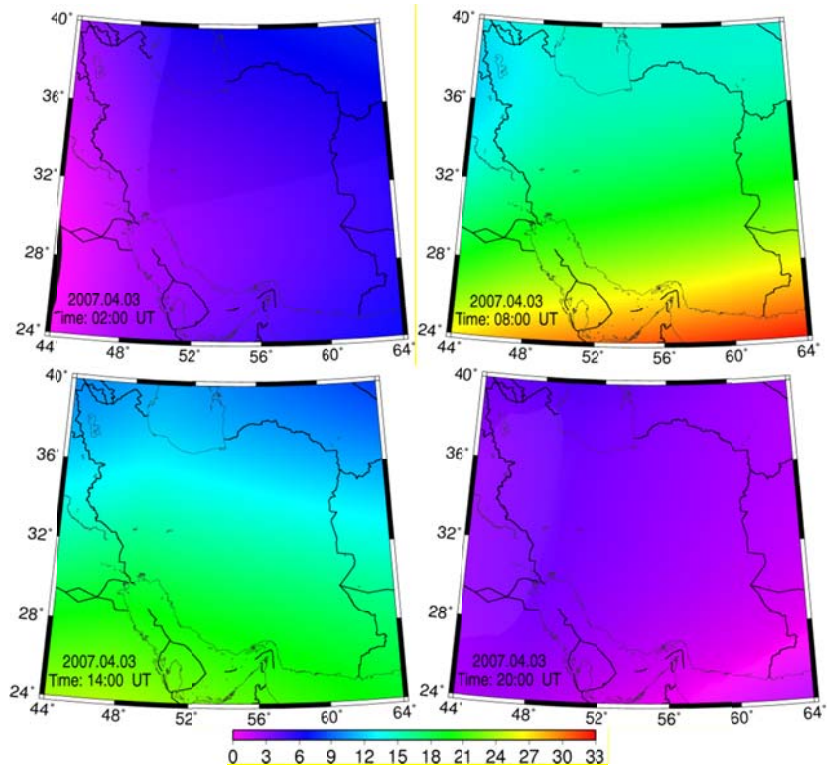

Figure 10. The model estimates of VTEC (10^{16} ele./m^2) at four times in 2007.04.03.

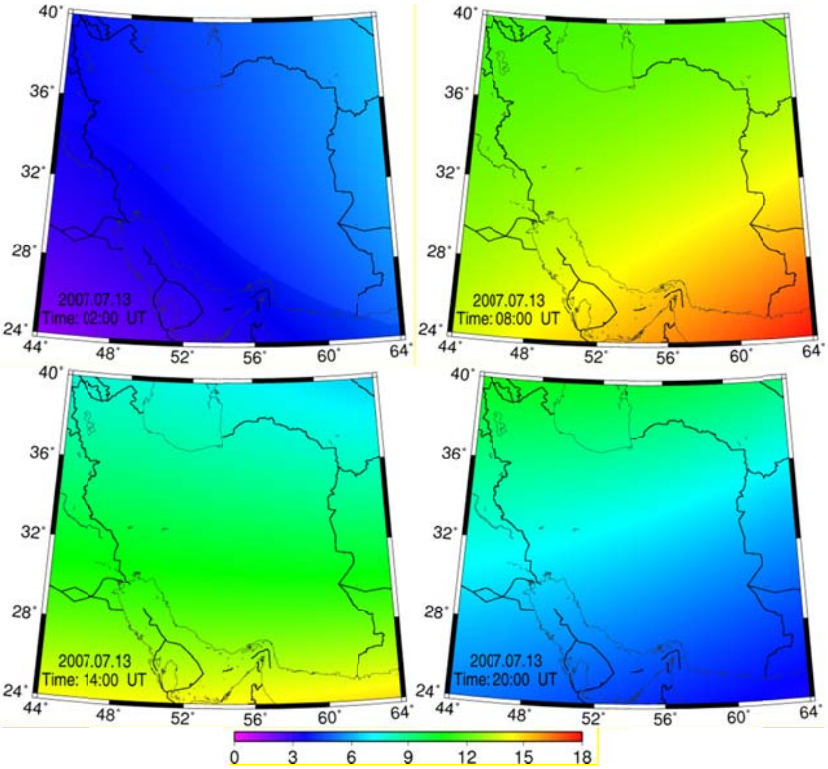

Figure 11. The model estimates of VTEC (10^{16} ele./m^2) at four times in 2007.07.13.

In Figures 9, 10 and 11 that are displayed for different times (two times in day-side and two times in night-side), it is clearly visible that the maximum electron density occurs during the day-side.

6. Discussion and conclusion

In this paper, voxel based ionospheric tomography was solved using artificial neural networks (ANNs). Three methods of ionospheric reconstruction were compared and evaluated. Residual minimization training neural network (RMTNN), modified RMTNN and ionospheric tomography based on the neural network (ITNN) were studied in this paper. In RMTNN method, standard ANN (SANN) with back-propagation (BP) training algorithm was used to reconstruct the ionosphere. Wavelet neural network (WNN) was used as base network in MRMTNN method. Besides, BP algorithm was used to train the network. In ITNN method, instead of BP algorithm and speed up of the convergence of the optimal solution, particle swarm optimization (PSO) algorithm was used. All three methods were evaluated using GPS and IGS data in Iran. The ionosonde data in Tehran (φ=35.73820, λ=51.38510) was used for validating the reliability of the proposed methods. Network structure, number of iteration and time of convergence to the optimal solution were compared in proposed methods. The time of convergence to the optimal solution and number of iteration in ITNN method was less than those of the MRMTNN and ITNN methods.

The RMSE and bias of ITNN method were less than the other two methods. It meant that by using WNN with PSO training algorithm, accuracy of the method was considerably increased. Moreover, the scatter plot for ionosonde electron density with corresponding electron density predictions from the three methods was computed. In this case, ionosonde electron density was highly correlated to ITNN with a correlation coefficient (R) of 0.9018 and lowest correlated with a correlation coefficient of 0.8264 in RMTNN. This study showed the superiority of the ITNN method over the other methods (RMTNN and MRMTNN). As a future research, this method is applicable for the reconstruction of the troposphere properties.

References

Amerian, Y., Mashhadi Hossainali, M., Voosoghi, B. and Ghaffari razin, M. R, 2010, Tomographic reconstruction of the ionospheric electron density in term of wavelets. Journal of Aerospace Science and Technology, 7(1), 19–29.

Austen, J. R., Franke, S. J. and Liu, C. H., 1988, Ionospheric imaging using computerized tomography. Radio Sci., 23, 299–307.

Alexandridis, A. and Zapranis, A., 2013, Wavelet neural networks: A practical guide. Neural Networks, 42 1–27.

Ghaffari Razin, M. R., 2015, Development and analysis of 3D ionosphere modeling using base functions and GPS data over Iran. Acta Geod. Geophys., DOI 10.1007/s40328-015-0113-9, 51(1) , 95-111.

Ghaffari Razin, M. R. and Voosoghi, B., 2016, Regional ionosphere modeling using spherical cap harmonics and empirical orthogonal functions over Iran. Acta Geod. Geophys., 52(1), 19-33, doi: 10.1007/s40328-016-0162-8.

Ghaffari Razin, M. R., Voosoghi, B. and Mohammadzadeh, A., 2015, Efficiency of artificial neural networks in map of total electron content over Iran. Acta Geod. Geophys., DOI 10.1007/s40328-015-0143-3.

Ghaffari Razin, M. R. and Voosoghi, B., 2016, Regional application of multi-layer artificial neural networks in 3-D ionosphere tomography. Advances in Space Research. http://dx.doi.org/10.1016/j.asr.2016.04.029.

Hirooka, S., Hattori, K. and Takeda, T., 2011, Numerical validations of neural-network-based ionospheric tomography for disturbed ionospheric conditions and sparse data. Radio Sci., 46(5), RS0F05, DOI: 10.1029/2011RS004760.

Habarulema, J. B., McKinnell, L.-A. and Opperman, B. D. L., 2009, A recurrent neural network approach to quantitatively studying solar wind effects on TEC derived from GPS; preliminary results, Ann. Geophys., 27, 2111–2125, doi:10.5194/angeo-27-2111-2009.

Kunitsyn, V. E., Nesterov, I. A., Padokhin, A. M. and Tumanova, U. S., 2011, Ionospheric Radio Tomography based on the GPS/GLONASS navigation systems. J. Commun. Technol. Electron., 56(11), 1269-1281, doi: 10.1134/S1064226911100147.

Kennedy, J. and Eberhart, R., 1995, Particle swarm optimization. Proceedings of the IEEE International Conference on Neural Networks, 4(ICNN ’95), 1942–1948, Perth, Western Australia, November-December 1995.

Liaqat, A., Fukuhara, M. and Takeda, T., 2003, optimal estimation of parameter of dynamical system by neural network collocation method. Comput. Phys. Commun., 150, 215–234, doi:10.1016/S0010-4655(02) 00680-X, 2003.

Ma, X. F., Maruyama, T., Ma, G. and Takeda, T., 2005, Three dimensional ionospheric tomography using observation data of GPS ground receivers and ionosonde by neural network. J. Geophys. Res., 110, A05308, doi: 10.1029/2004JA010797.

Pokhotelov, D., Jayachandran, P., Mitchell, C. N., MacDougall, J. W. and Denton, M. H., 2011, GPS tomography in the polar cap: comparison with ionosondes and in situ spacecraft data. GPS Solut., 15(1), 79–87. doi:10.1007/s10291-010-0170-z.

Quarteroni, A., Sacco, R. and Saleri, F., 2007, Numerical Mathematics, 37, Texts in Applied Mathematics, 2nd ed., Springer Berlin Heidelberg, Heidelberg, Germany.

Van de Kamp, M. M. J. L., 2013, Medium-scale 4-D ionospheric tomography using a dense GPS network. Ann Geophys., doi:10.5194/angeo-31-75-2013.

Wen, D. B., Wang, Y. and Norman, R., 2012, A new two-step algorithm for ionospheric tomography solution. GPS Solut., 16(1), 89–94, Jan./Feb.

Yilmaz, A., Akdogan, K. E. and Gurun, M., 2009, Regional TEC mapping using neural networks. Radio Sci., 44, RS3007, doi:10.1029/2008RS004049.

Yizengaw, E., Moldwin, M. B., Dyson, P. L. and Essex, E. A., 2007, Using Tomography of GPS TEC to Routinely

Determine Ionospheric Average Electron Density Profiles. Journal of Atmospheric and Solar-Terrestrial Physics, 69, 314-321.

Zhang, Q. and Benveniste, A., 1992, Wavelet Networks. IEEE Trans. Neural Networks, 3(6), 889–898.